Acta Biomaterialia 97 (2019) 657–670

Contents lists available at ScienceDirect

Acta Biomaterialia

journal homepage: www.elsevier.com/locate/actabiomat

Full length article

# Long-term *in vivo* study of biodegradable Zn-Cu stent: A 2-year implantation evaluation in porcine coronary artery

Chao Zhou [a,b,c,1], Hua-Fang Li [a,1], Yu-Xia Yin [a,c], Zhang-Zhi Shi [a], Ting Li [a], Xiang-Yi Feng [c], Jun-Wei Zhang [c], Cai-Xia Song [c], Xiao-Shan Cui [c], Kai-Li Xu [c], Yan-Wei Zhao [c], Wen-Bo Hou [c], Shou-Tao Lu [c], Guang Liu [c], Mao-Quan Li [b], Jian-ying Ma [d], Egon Toft [e], Alex A. Volinsky [f], Min Wan [g], Xiu-jun Yao [g], Chang-bin Wang [g], Kang Yao [d], Shi-kun Xu [d], Hao Lu [d], Shu-Fu Chang [d], Jun-Bo Ge [d,*], Lu-Ning Wang [a,*], Hai-Jun Zhang [b,c,h,*]

[a] *Beijing Advanced Innovation Center for Materials Genome Engineering, School of Materials Science and Engineering, University of Science and Technology Beijing, Beijing 100083, PR China*
[b] *Department of Interventional and Vascular Surgery, The Tenth People's Hospital of Shanghai, Tongji University, Shanghai 200072, PR China*
[c] *National United Engineering Laboratory for Biomedical Material Modification, Branden Industrial Park, Qihe Economic & Development Zone, Dezhou City, Shandong 251100, PR China*
[d] *Shanghai Institute of Cardiovascular Diseases, Zhongshan Hospital, Fudan University, 180 Fenglin Road, Shanghai 200032 PR China*
[e] *Biomedical Research Center, College of Medicine, Qatar University, Shareh Jamiaa, Post Box 2716, Doha, Qatar*
[f] *Department of Mechanical Engineering, University of South Florida, Tampa, FL 33620, USA*
[g] *Shandong Quality Inspection Center for Medical Devices, No. 15166 Century Avenue, Jinan H-T Industrial Development Zone, Shandong 250101, PR China*
[h] *Department of Health Science and Technology, Faculty of Medicine, Aalborg University, Niels Jernes Vej 10, Aalborg Ø 9220, Denmark*

ARTICLE INFO

*Article history:*
Received 25 March 2019
Received in revised form 11 July 2019
Accepted 6 August 2019
Available online xxxx

*Keywords:*
Zn-based biodegradable stent
Coronary artery stent
Biodegradation performance
*In vivo* evaluation
Medical device performance

ABSTRACT

In the present study, a novel biodegradable Zn-0.8Cu coronary artery stent was fabricated and implanted into porcine coronary arteries for up to 24 months. Micro-CT analysis showed that the implanted stent was able to maintain structural integrity after 6 months, while its disintegration occurred after 9 months of implantation. After 24 months of implantation, approximately 28 ± 13 vol% of the stent remained. Optical coherence tomography and histological analysis showed that the endothelialization process could be completed within the first month after implantation, and no inflammation responses or thrombosis formation was observed within 24 months. Cross-section analysis indicated that the subsequent degradation products had been removed in the abluminal direction, guaranteeing that the strut could be replaced by normal tissue without the risk of contaminating the circulatory system, causing neither thrombosis nor inflammation response. The present work demonstrates that the Zn-0.8Cu stent has provided sufficient structural supporting and exhibited an appropriate degradation rate during 24 months of implantation without degradation product accumulation, thrombosis, or inflammation response. The results indicate that the Zn-0.8Cu coronary artery stent is promising for further clinical applications.

**Statement of Significance**

Although Zn and its alloys have been considered to be potential candidates of biodegradable metals for vascular stent use, by far, no Zn-based stent with appropriate medical device performance has been reported because of the low mechanical properties of zinc. The present work presents promising results of a Zn-Cu biodegradable vascular stent in porcine coronary arteries. The Zn-Cu stent fabricated in this work demonstrated adequate medical device performance both *in vitro* and *in vivo* and degraded at a proper rate without safety problems induced. Furthermore, large animal models have more cardiovascular similarities as humans. Results of this study may provide further information of the Zn-based stents for translational medicine research.



* Corresponding authors at: Beijing Advanced Innovation Center for Materials Genome Engineering, School of Materials Science and Engineering, University of Science and Technology Beijing, Beijing 100083, PR China (L.N. Wang) and Department of Interventional and Vascular Surgery, The Tenth People's Hospital of Shanghai, Tongji University, Shanghai 200072, PR China (H.J. Zhang).
*E-mail addresses:* ge.junbo@zs-hospital.sh.cn (J.-B. Ge), luning.wang@ustb.edu.cn (L.-N. Wang), zhanghaijun@tongji.edu.cn (H.-J. Zhang).
[1] These authors contributed equally to this work.

https://doi.org/10.1016/j.actbio.2019.08.012
1742-7061/

## 1. Introduction

Coronary artery stenting (CAS) is currently the most reliable therapy to treat coronary artery disease [1]. Patients who were implanted with permanent coronary stents have to bear them for the rest of their life. Late-stage thrombosis [2] and chronic inflammation [3] related to the permanent stented segment continue to accrue. Evidence suggests that atherosclerosis accelerated by the permanent stent is an important underlying mechanism of these late adverse events [4]. Additionally, the existing permanent stents restrain the target vessel and impair the coronary vasomotion. The stent embedded in the vessel acts as a "cage," which may impede bypass grafting operation [5].

Zinc (Zn) has been recently listed as a novel bioabsorbable stent candidate material owing to its near-ideal degradation rate and acceptable biocompatibility [6]. Zn is the second most abundant trace metal in higher animals and affects major metabolic processes, as well as regulation of the cell cycle [7]. It also plays positive roles in the prevention of heart disease, such as maintaining the integrity of endothelial cells (EC) [8], stimulating the proliferation of EC through increasing the levels of endogenous basic fibroblast growth factor [9], and improving cardiac function, as well as preventing further damage such as that caused by ischemia and infarction [10].

Recent *in vivo* studies of pure zinc stent (rabbit abdominal aorta) [6] show considerable promise of the zinc-based stents as fully biodegradable coronary stent candidates (with no severe signs of inflammation, intimal hyperplasia, and thrombosis formation).

Nevertheless, the poor mechanical properties of the pure Zn are far below the requirements of a potential biodegradable metal for vascular stent use. Adding alloying elements is one of the most effective methods for improving the poor mechanical properties of pure Zn. Elements such as Mg, Ca, Sr, Ge, Ag, and Mn have already been chosen as alloying elements for developing biodegradable Zn-based alloys with enhanced mechanical properties [11–15].

Copper, which is an important essential element to the body [16], can induce vascular endothelial growth factor (VEGF) expression [17] and positively influence the re-endothelialization of vascular endothelium and the maintenance of endothelial function. The intact endothelium is considered to be important for reducing the risks of coronary endothelial dysfunction distal to the stent [18], which is an independent predictor of atherosclerotic disease progression and cardiovascular event rates [19]. Additionally, previous studies have investigated the practice of adding copper in medical devices for antibacterial and angiogenesis functions [20–24]. Several Zn-Cu alloy systems have also been developed as potential biomedical materials [25,26].

However, these previous studies focused only on the *in vitro* material characterization of the alloys, and neither *in vitro* nor *in vivo* medical device performance of the Zn-Cu alloys has been reported. In the present work, a novel biodegradable Zn-0.8Cu (wt.%) coronary stent was fabricated and implanted into porcine coronary arteries for 24 months. Characterization of mechanical properties and quantitative coronary angiography (QCA) were carried out to evaluate the *in vitro* and *in vivo* performance of the medical device. Optical coherence tomography (OCT), micro-computed tomography (Micro-CT), histopathological observations, scanning electron microscopy (SEM), and energy-dispersive spectrometry (EDS) were performed to investigate the degradation behavior and biocompatibility of the Zn-0.8Cu stents.

## 2. Materials and methods

### 2.1. Preparation of the Zn-0.8Cu stent

Micro-tubes with an outer diameter of 1.575 mm and wall thickness of 127 μm were used to fabricate the Zn-Cu stent (for detailed information about the stent fabrication processes, refer to S1). The Cu content of the micro-tube was evaluated using an inductively coupled plasma atomic emission spectrometer (ICP-AES; iCAP7600, Thermo Fisher Scientific, USA), showing (0.80 ± 0.01) wt%, which is close to the nominal composition. Phase composition analysis of the stent was carried out on the micro-tubes using an X-ray diffractometer (XRD, Rigaku, SmartLab, Japan) with Cu Kα radiation with 2θ ranging from 10° to 90° at a 1°/min scanning rate.

After femtosecond laser cutting (S1.2, Fig. S2a), the acid pickling process was carried out in 2% $H_2SO_4$ solution for 20 s in an ultrasonic cleaner; afterwards, the stents were cleaned with distilled water and dried in a vacuum oven (Fig. S2b). The polishing solvent for chemical polishing processes is mainly composed of 100 ml/L 67% $HNO_3$, 20 ml/L glycerol, 20 ml/L $H_2SO_4$, and a small amount of $CrO_3$. Stents were then immersed in the polishing solvent for approximately 1 min to obtain the final wall thickness of (0.10 ± 0.01) mm and immediately transferred to distilled water to terminate the reaction. Finally, the Zn-Cu stents were washed twice in the ultrasonic cleaner using distilled water (each time for 20 s), dried, and stored in a vacuum oven (Fig. S2c and Fig. 1a). Crimping (Fig. 1b), packaging, and ethylene oxide sterilization were carried out subsequently. All processes mentioned above were supported by Rientech MedTec Co., Ltd.

### 2.2. Medical device performance of the Zn-Cu stent

#### 2.2.1. Integrity and crossing profile of the Zn-Cu stent

After chemical polishing, crimping, and expanding processes were carried out under human body temperature condition (37 °C). The micro-morphology of the Zn-Cu stent was recorded using a stereomicroscope (Leica, S4 E, Germany) to evaluate the integrity of the Zn-Cu stents during the process of chemical polishing, crimping, inflation to a nominal diameter, and further balloon burst. The outer diameter of the stent, when crimped onto a stent delivery system (SDS), was evaluated as the crossing profile of the stent.

#### 2.2.2. Radial strength of the Zn-Cu stent

Zn-Cu stents (n = 3) were first inflated to the nominal diameter (3.0 mm of the balloon) by the SDS and released under human body temperature. Then the curves of radial load vs. compressive diameter were constructed at a compression rate of 0.1 mm/s using a radial strength tester (Blockwise, TTE2, USA). The radial strength (kPa) of the stents was defined as the strength at 10% compression of the initial compression diameter ($D_0$).

#### 2.2.3. Radiopacity of the Zn-Cu stent

The radiopacity of the stents was evaluated by the visibility of angiographic images. The angiographic images of the Zn-Cu stent during the implantation and repeated QCA (GE Medical, Innova 2000, USA) processes were recorded (see 2.3 and 2.4).

### 2.3. Implantation process

Animal experiments were approved by the Animal Ethics Committee of the Zhongshan Hospital, Fudan University (Permit

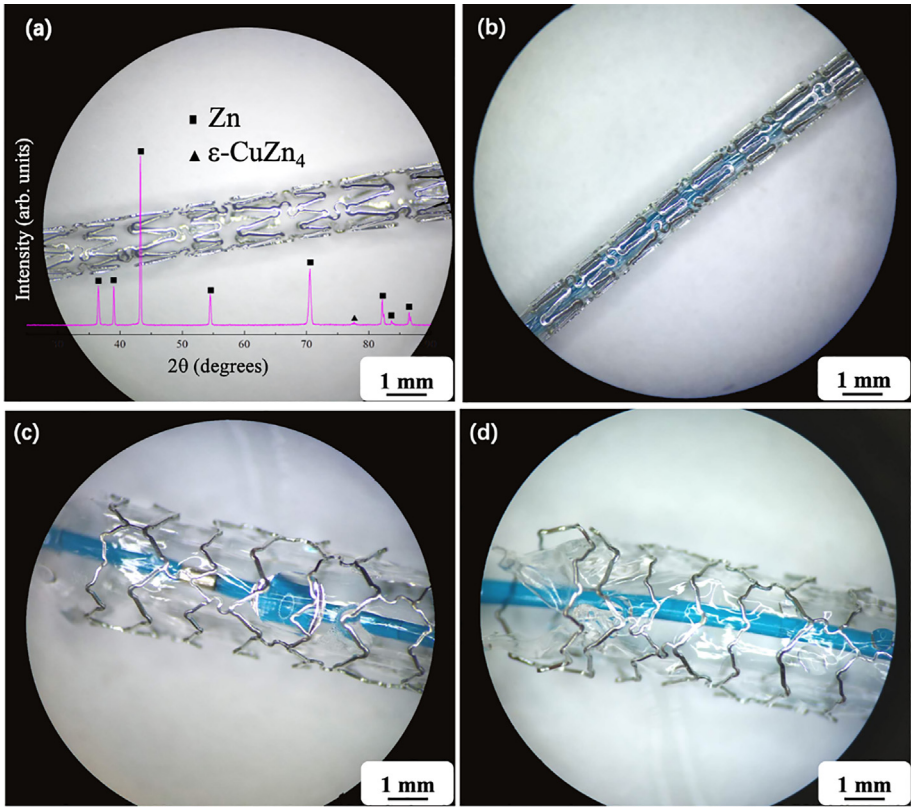


**Fig. 1.** Surface morphology of the Zn-Cu stent (a) after chemical polishing; (b) after crimping; (c) inflated to nominal pressure; (d) inflated to balloon-burst. The insert of (a) is the XRD pattern of the Zn-Cu stent.

Number: 16-0406), and carried out under the National Institutes of Health Guide for Care and Use of Laboratory Animals.

Sixteen healthy female Shanghai white pigs (purchased from Shanghai Jiagan Biotechnology Co. Ltd., 6 months old, weighing 40–50 kg) were used in this study. Two or three stents were implanted in each of the pigs in the left anterior descending artery (LAD), left circumflex artery (LCX), or right coronary artery (RCA). Finally, 40 Zn-Cu stents were implanted. For each time point, desired numbers of stented vessels (6 vessels in 2–3 pigs) underwent repeated QCA process (GE Medical, Innova 2000, USA), and the animals were then sacrificed if sampling processes were needed. 3 samples were used for the micro-CT and histology analysis, 3 samples used for SEM and EDS analysis at each time point.

Aspirin (100 mg/day) and clopidogrel (75 mg/day) intake was started 3 days before angioplasty and continued until sacrifice. All pigs fasted overnight before the stent implantation procedure. Then they were sedated by an intramuscular injection of 20 mg/kg ketamine, 2 mg/kg xylazine, and 0.05 mg/kg atropine. After intubation, general anesthesia was induced and maintained with isoflurane (2.5%).

The implantation procedure was carried out using the endovascular stent puncture technology through the femoral artery. The coronary segments were selected from LAD, LCX, or RCA to obtain a stent/artery ratio of 1.1. Additional inflations were performed based on the target site diameter. In each group, two or three stents were positioned in one pig and only one stent was placed in a single artery. The electrocardiogram and blood pressure were monitored during the operation.

The diameter of reference vessel, instant diameter (when the balloon was inflated), and post-implantation diameter (immediately after the deployment system was removed) on target vessel were measured using the internal digital calipers of the fluoroscope with the guiding catheter serving as a reference for calibration (QCA, GE Medical, Innova 2000, USA). Compression hemostasis was adopted to prevent hematoma formation at the puncture site after implantation.

### 2.4. Micro-CT analysis

Euthanization of pigs was immediately followed by perfusion and fixation of the stented coronary artery with 10% buffered formalin. Micro-CT (Bruker, SkyScan 1172, Belgium) 3D reconstruction was performed by N-Recon after the fixation process to evaluate the degradation properties of the stents implanted in the porcine coronary arteries. For each time interval (3, 6, 9, 12, 18, and 24 months), three Zn-0.8Cu stents with vessel tissue were examined (spatial resolution of pixel size 35 μm; X-ray tube voltage of 65 kV; anode current of 370 mA; 1 mm Al filter; and 0.70° rotation step over 180°). Reconstruction and volume analysis of the stent residuals were performed using CT-Vox Software (Bruker, SkyScan, Belgium).

The micro-CT volume analysis is grayscale-based. Different densities of materials are observed as different grayscales: the residual of the Zn-0.8Cu struts was observed with a grayscale of 80–250, the tissues were observed with a grayscale of 0–20, and the degradation products were observed with a grayscale of 20–80.

### 2.5. QCA and OCT test

The pigs underwent repeated QCA (GE Medical, Innova 2000, USA) after 1, 3, 6, 9, 12, 18, and 24 months of implantation to measure the minimal lumen diameter (MLD) of target vessels (with heparin as an anticoagulant). Late lumen loss (LLL) was then calculated using the MLD (LLL = MLD – (post-implantation instant diameter)). After the follow-up, angiographic observation, optical coherence tomography (OCT, St. Jude Medical, C7 XR LightLab

Imaging, USA) was carried out to investigate the neointima and thrombosis post-stenting. After repeated QCA and OCT tests, pigs were euthanized at sacrifice time points.

### 2.6. Cross-sectional analysis

For cross-sectional analysis, the stented artery segments were embedded with methyl methacrylate (MMA). Sections of 50 μm thickness were cut in the coronal plane using a Leica SP1600 saw microtome (Leica Microsystems, SP1600, Canada) for hematoxylin-eosin (H&E) staining. The stained cross-sections were observed using a Leica DM LB2 bright-field microscope (Leica, DM LB2, Germany). The morphology of the cross-sections was observed using a SEM (Hitachi, SU8010, Japan). Analysis for elemental composition determination in local areas, line analysis, and mapping analysis of the stent–tissue interface were performed using EDS (Horiba, EMAX 6853-H, Japan).

### 2.7. Zn element accumulation analysis

At time points of 6, 12, and 24 months, a desired volume of the apex cordis was sampled at the distal and proximal ends 5 mm away from the stented artery segments, and the wet weight was immediately weighed. Samples were liquid nitrogen-preserved before the Zn element was analyzed using an inductively coupled plasma atomic emission spectrometer (ICP-AES, Thermo Fisher Scientific, iCAP7600, USA).

### 2.8. Statistical analysis

Statistical analysis was performed with the SPSS 18.0 software package (SPSS Inc., Chicago, USA). Group means were calculated and compared by the analysis of variance and the *t*-test. Results were reported as "mean value" ± SD. Differences among groups were significant with the p-value <0.05 (two-tailed).

## 3. Results

### 3.1. Intraoperative and postoperative monitoring

Forty Zn-Cu stents were implanted in 16 pigs. Neither abnormal electrocardiogram nor abnormal blood pressure was observed during the operation. The anesthesia was maintained steadily. Perforation of coronary sinus, cardiac tamponade, or thrombus formation did not occur. Hematoma had been avoided by the adoption of compression hemostasis (more than 30 min). The pigs woke up from the anesthetic state 2–3 h postsurgery. On the day immediately after the operation, the pigs were fed with water when they returned to the feeding room, and they were allowed to have regular food in the next few days.

### 3.2. Medical device performance of the Zn-Cu stent

#### 3.2.1. Integrity and crossing profile of the Zn-Cu stent

Fig. 1a shows a representative surface morphology image of the Zn-Cu stent after chemical polishing. The insert of Fig. 1a shows an XRD pattern of the Zn-Cu stent, which shows that the phase composition of the Zn-Cu stent is a Zn matrix and a metastable secondary ε phase (ε-$CuZn_4$). Fig. 1b–d show that the Zn-Cu stent can retain its integrity during (b) the crimping process, (c) inflating process, and even when inflated to (d) balloon burst. The Zn-Cu stent possesses a crossing profile value of 0.8–1.0 mm.

#### 3.2.2. Radial strength of the Zn-Cu stent

Fig. 2 shows the radial compression curves of the Zn-Cu stent. The radial strength the Zn-Cu stents is (114 ± 3) kPa.

#### 3.2.3. Radiopacity

Fig. 3 shows the angiographic images of (a) the Zn-Cu stent during the stenting procedure and (b) the Zn-Cu stent after 18 months of implantation. Fig. 3a shows that the radiopacity of the Zn-Cu stent is quite clear during the implantation process. Fig. 3b shows that the Zn-Cu stent becomes invisible under X-ray during the repeated QCA of 18 months, which was contributed by the degradation of the material.

### 3.3. Degradation process observation by micro-CT

Micro-CT images at each time point are shown in Fig. 4. Fig. 4a shows the 3D Micro-CT image of the Zn-Cu stent before implantation. Fig. 4b indicates that the degradation of the stent is quite uniform with no localized accumulation of degradation products after implantation for 3 months. A compact and continuous corrosion layer is observed in Fig. 4b-4d, which indicates that the dominant corrosion type is still uniform corrosion after 9 months of implantation. As shown in Fig. 4c, the Zn-Cu stent can maintain the

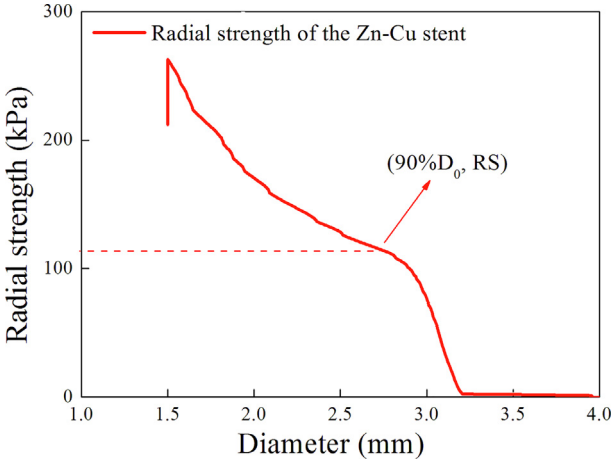


**Fig. 2.** Radial strength of the Zn-Cu stent. RS (radial strength) is defined as the strength of 10% compression of the initial compression diameter ($D_0$).

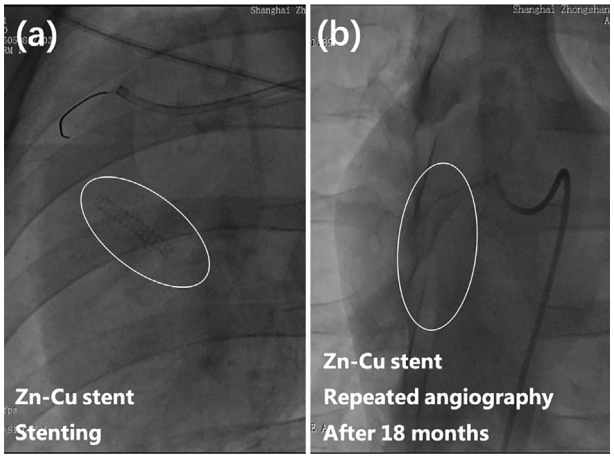


**Fig. 3.** Radiopacity of the Zn-Cu stent (highlighted by white circles): (a) Zn-Cu stent in a porcine coronary artery during the stenting procedure; (b) Zn-Cu stent in a porcine coronary artery after 18 months of implantation.

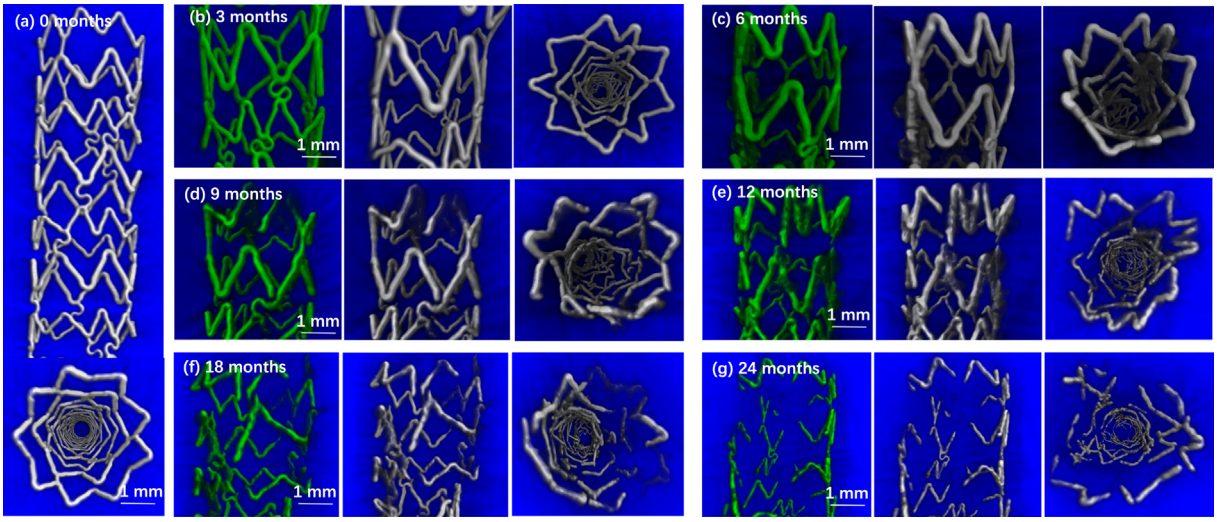


**Fig. 4.** (a) 3D Micro-CT image of the Zn-Cu stent before implantation; selected 3D micro-CT images after (b) 3, (c) 6, (d) 9, (e) 12, (f) 18, and (g) 24 months of implantation. Each time point is composed of three images: the green one represents degradation products (front view); the white ones are combinations of residual zinc and degradation products (front views in the middle and top views in the right). (For interpretation of the references to colour in this figure legend, the reader is referred to the web version of this article.)

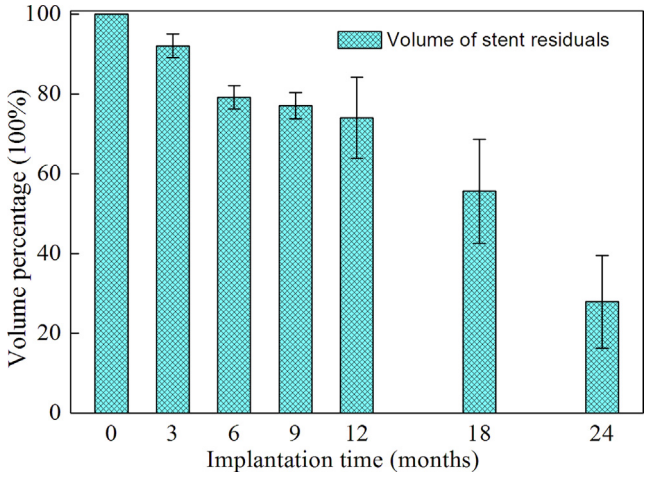


**Fig. 5.** Volume change of the stent residuals. The residuals of the Zn-Cu stents were observed with a grayscale of 80–250.

mechanical integrity for at least 6 months post-implantation. A few localized corrosion positions in the struts can be found at this time point. As shown in Fig. 4d, fractures in the curved places of the struts occurred. Severe disintegration of the stent structure occurred at 12 months (Fig. 4e), at which point there were almost no integrated support units found. Fig. 5 shows the volume change of the stent residuals. The residual volume of the Zn-Cu stent at 3, 6, 9 12, 18, and 24 months is (92 ± 1)%, (79 ± 4)%, (77 ± 4)%, (74 ± 12)%, (56 ± 19)%, and (28 ± 13)%, respectively.

### 3.4. H&E analysis

H&E-stained cross-sections at time points of 1, 3, 9, and 24 months are shown in Fig. 6. As shown in Fig. 6a and Fig. 6a1, the endothelialization process completes within the first month of the post-surgery process, and the struts are tightly integrated with the neointima and surrounding tissues. Accumulation of the macrophages around the struts is found after 3 months of implantation, as shown in Fig. 6b and Fig. 6b1. Macrophage infiltration decreased after the 9 months of implantation and turned into a mild inflammation, as observed in Fig. 6c and Fig. 6c1. Fig. 6c1 shows a part-degraded strut, which has been partially replaced by smooth muscle cells (SMC) similar to native ones.

The area highlighted by the green square in Fig. 6d1 is the former position of a partially degraded strut, which has been mostly replaced by SMC, without serious inflammation. Degradation products are observed near the former place, which can be seen to be diffused in the abluminal direction. Fig. 6d2 was obtained by overexposure, in which the black arrows marked the strut residuals and the degradation products' debris around the struts. The green circle in Fig. 6d3 highlights a multinucleated giant cell that carried one part of the degradation products.

### 3.5. Results of QCA

All stented vessel segments in this study were statistically analyzed to evaluate the acute recoil (40 stented segments), which was thought to be an important factor for stent medical device performance. The rate of acute recoil for Zn-Cu stents ((4 ± 3) %) is listed in Table 1.

The MLD directly reflects the ability of blood to pass through the vessel (smaller MLD represents poorer capacity); therefore, it is an important parameter to evaluate the reconstruction of blood flow for the stented vessel. LLL, which is calculated using the MLD (LLL = MLD – (post-implantation instant diameter)), is an important mechanistic observation to characterize the behavior of the stent [27,28]. Fig. 7 shows the MLD results evaluated by QCA. Relative MLD and LLL data are listed in Table 2. The inserts of Fig. 7 (a)–(c) are 3D images of the stent residuals at time points of 0, 12, and 24 months of reconstruction through micro-CT, respectively.

### 3.6. OCT results

Fig. 8a–f are section images of the stented vessel segments. The bright points distributed on the circumference with black shadows behind are the stent struts. Inside the struts is the newborn endomembrane. Fig. 8(a) shows that there is a complete newborn endomembrane inside the stent, which means the endothelialization process has completed within 1 month after implantation. The struts observed by OCT have become increasingly obscure with the degradation of the Zn-Cu stents, and at the endpoint of this

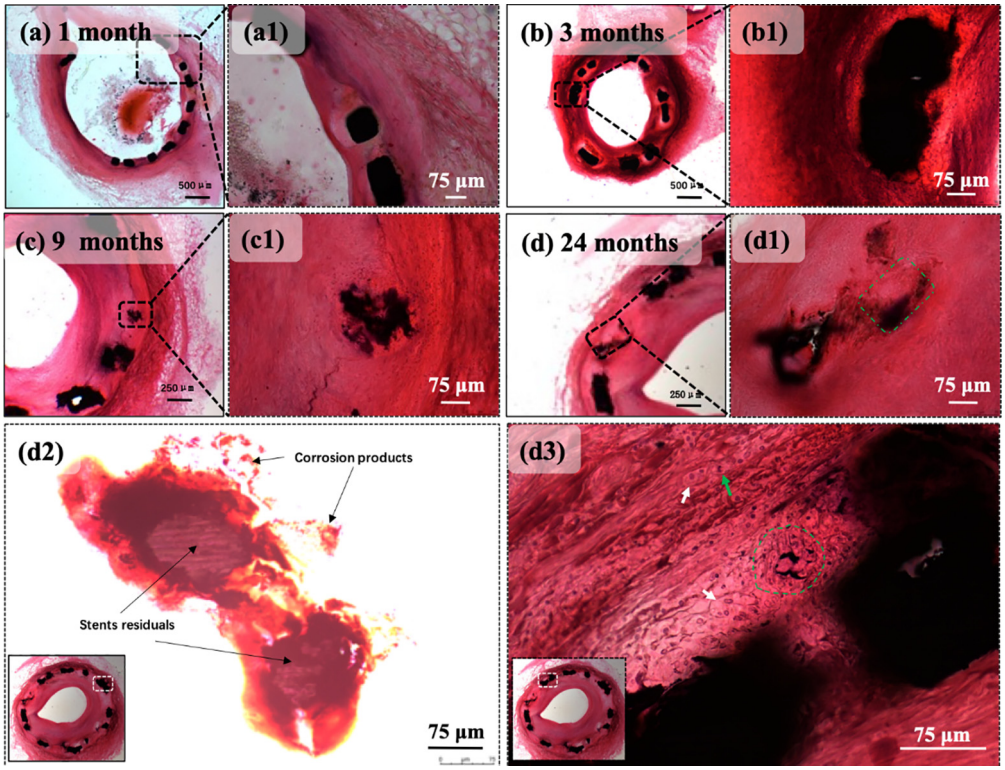


**Fig. 6.** H&E-stained cross-sections of the selected segments at time points of (a) 1 month, (b) 3 months, (c) 9 months, and (d) 24 months; (a1), (b1), and (c1) are the partially enlarged images of (a), (b), and (c), respectively; (d1), (d2), and (d3) are the partially enlarged images of (d); (d1) Green square marks the former position of a strut, which has been replaced by smooth muscle cells; (d2) the image obtained by overexposure, in which the strut residuals and the degradation products (marked by black arrows) can be clearly seen; (d3) white arrows mark the epithelioid cells, green arrow marks lymphocytes, green circle highlights a foreign body-type giant cell with degradation products of the 10–15 μm size. (For interpretation of the references to colour in this figure legend, the reader is referred to the web version of this article.)

**Table 1**
Acute recoil of the Zn-Cu stent (sample number: 40).

| Reference vessel diameter (mm) | Instant vessel diameter (mm) | Instant diameter after implantation (mm) | Acute lumen loss (recoil) |
|---|---|---|---|
| 2.8 ± 0.3 | 3.1 ± 0.2 | 3.0 ± 0.2 | (4 ± 3) % |

study, the struts became almost invisible in the OCT images (Fig. 8f). The newborn endomembrane was smooth, and no thrombosis was observed until the end of the study period (Fig. 8g).

### 3.7. SEM and EDS analyses

Fig. 9 shows the line analysis results of the selected cross-sections at time points of 1, 3, 9, and 18 months. At each time point, three representative regions could be recognized in the SEM images. The first one was the Zn-Cu strut, and only Zn and Cu signals were found in this region. The second one was the degradation product, which was observed around the Zn-Cu struts and had a remarkable Zn, Cu, O, Ca, and P enrichment. The third one was tissue, which showed an evident signal of C, without Zn

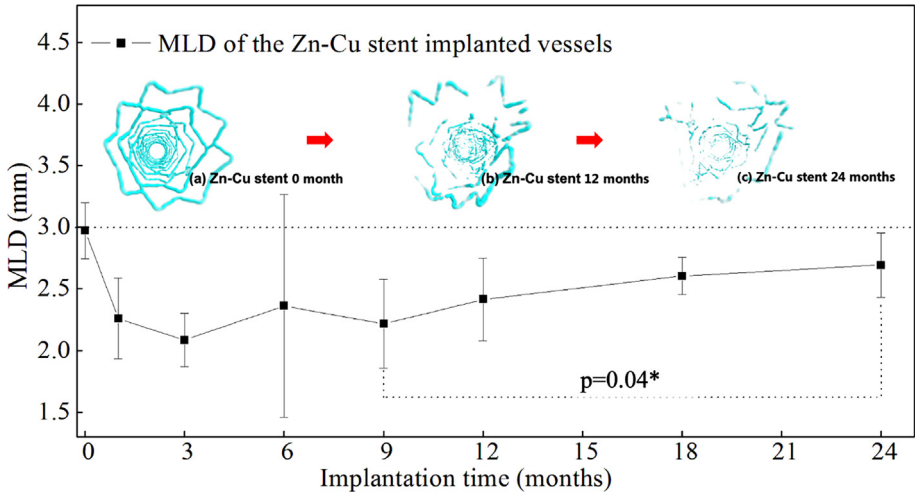


**Fig. 7.** MLD of Zn-Cu stented vessels at each time point (n = 6). The insets are Micro-CT 3D images (top view) of (a) the Zn-Cu stent before implantation; (b) the Zn-Cu stent residuals after 12 months; and (c) the Zn-Cu stent residuals after 24 months. The symbol "*" indicates that the difference between the MLD value at 9 and 24 months is significant.

**Table 2**
Minimal lumen diameter (MLD) and late lumen loss (LLL) of the Zn-Cu stented vessels (sample number: 6).

| Time points | 1 month | 3 months | 6 months | 9 months | 12 months | 18 months | 24 months |
|---|---|---|---|---|---|---|---|
| MLD at each time point (mm) | 2.3 ± 0.33 | 2.1 ± 0.2 | 2.4 ± 0.9 | 2.2 ± 0.4 | 2.4 ± 0.3 | 2.6 ± 0.2 | 2.7 ± 0.3 |
| Late lumen loss (mm) | 0.7 ± 0.4 | 0.9 ± 0.3 | 0.8 ± 0.2 | 0.5 ± 0.3 | 0. 6 ± 0.6 | 0.6 ± 0.5 | 0.3 ± 0.4 |

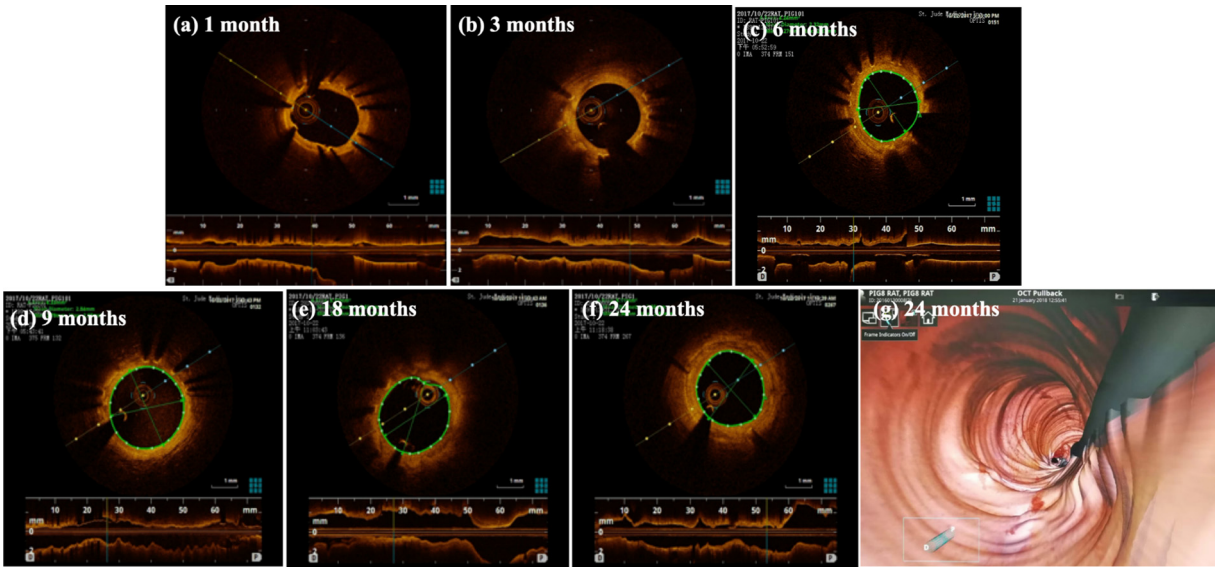


**Fig. 8.** OCT images of Zn-Cu stented vessels at each time point. Sectional images of the Zn-Cu stent-implanted vessel segments acquired at time points (a) 1, (b) 3, (c) 6, (d) 9, (e) 18, and (f) 24 months. (g) Shows the 3D image (top view) of the newborn endomembrane of the Zn-Cu stent-implanted vessel segment at 24 month time point.

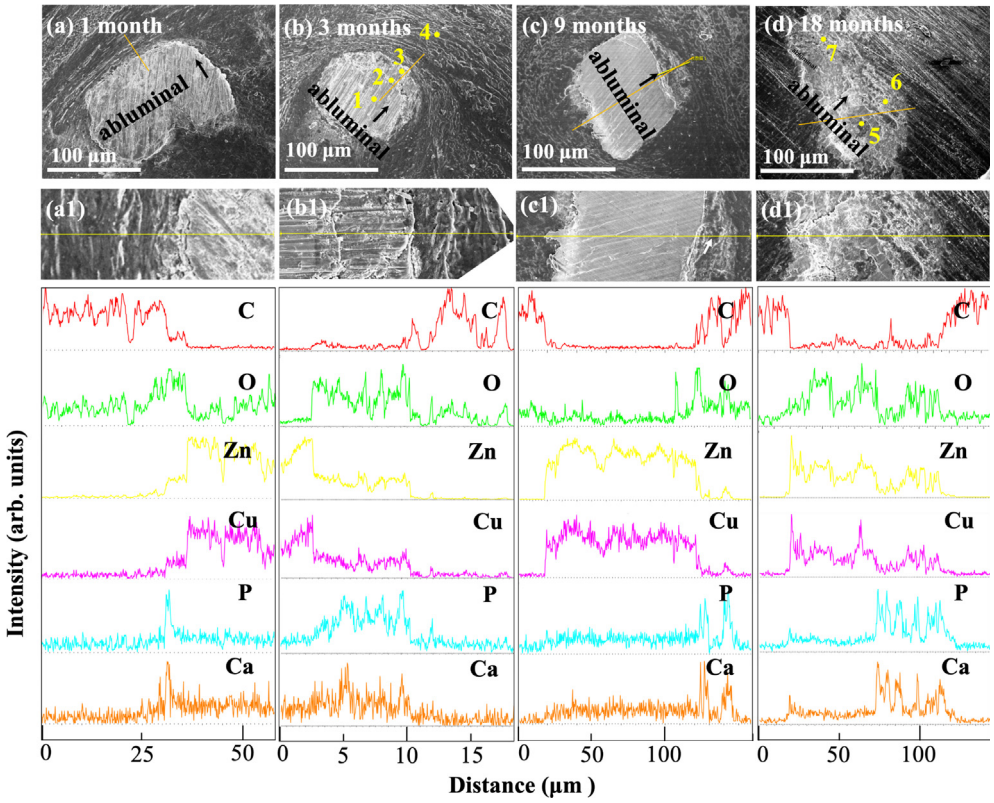


**Fig. 9.** SEM images of the cross-section at (a) 1, (b) 3, (c) 9, and (d) 18 months; (a1), (b1), (c1), and (d1) are the partial enlarged images of (a), (b), (c), and (d), respectively. Yellow bars in the SEM images mark the scanning area of the line analysis. Yellow points in SEM images (b) and (d) mark the analyzed points. Black arrows in the SEM images mark the abluminal direction. White arrow in (c1) marks the tissue between the strut and the degradation products. The curves below the SEM images show the elemental distribution of C, O, Zn, Cu, P, and Ca along the line scan shown in each figure. (For interpretation of the references to colour in this figure legend, the reader is referred to the web version of this article.)

and Cu peaks. The white arrow in Fig. 9c1 marks a place where the degraded struts were replaced by normal tissues. Fig. 9d shows a fully degraded Zn-Cu strut area with only degradation products remained *in situ*.

Fig. 10 shows SEM images and elemental mapping of the selected segments. A uniform thin corrosion product layer with remarkable P enrichment could be observed around the strut in Fig. 10a. As shown in Fig. 10b, the corrosion product layer became thicker in the abluminal direction, and the Ca signal in the layer could be observed more clearly. The white arrow in Fig. 10c marks a place where the degraded struts were replaced by normal tissues. Fig. 10d shows that the degradation products have diffused into the nearby tissues after 18 months of implantation.

Table 3 lists the elemental analysis results of the yellow points in Fig. 9b and Fig. 9d. Points 1 and 4 represent the stent residuals and tissues, respectively. Analysis results of points 2, 3, 5, 6, and 7 show the element content of the degradation products. Point 2 represents the initial degradation products around the struts, which had a lower Ca and P content and a higher Zn and Cu content. Point 7 may be a typical sequential degradation product, which has a higher Ca and P content and a lower Zn and Cu content. The ratio of Zn/Ca in the degradation products can change in a wide range from 321.2 at point 2 to 2.80 at point 7. These results suggest a replacement of the calcium phosphate to zinc phosphate with the degradation process progressing. The ratio of Ca/P in the most Ca-enriched degradation products (observed at point 7) is 0.61.

### 3.8. Accumulation analysis of Zn

The concentration of Zn in apex cordis, which is 5 mm away from the distal and proximal ends of the stented artery segments, is listed in Table 4. No significant difference was found between the Zn-Cu group and the negative control group.

## 4. Discussion

### 4.1. Medical device performance of the Zn-Cu stent

Surface roughness is an important factor of thrombogenicity and tissue reaction, and a smooth surface can help to prevent the activation and aggregation of platelets [29,30]. Fig. 1a indicates that the Zn-Cu stents developed in this work can be polished to an acceptable level ($R_a$ = 160 nm, described in S2.1) which is comparable to the commercialized stents (77–188 nm) [31].

As the premise of a balloon-expandable stent, the Zn-Cu stent has to withstand large-scale plastic deformations. This guarantees the stent can remain its integrity during the production and implantation processes. We can observe in Fig. 1b and 1c that

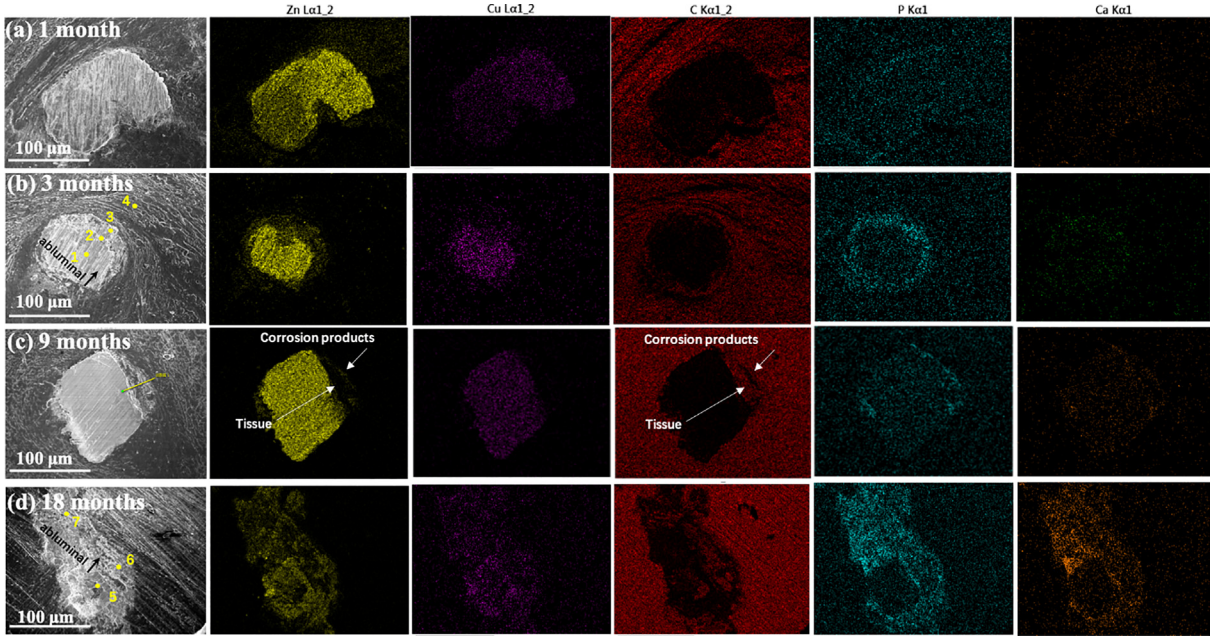


**Fig. 10.** Elemental mapping of the selected segments at time points of (a) 1 month; (b) 3, (c) 9, and (d) 18 months. Yellow points in SEM images (b) and (d) mark the analyzed points with the results shown in Table 3. Black arrows in the SEM images mark the abluminal direction. (For interpretation of the references to colour in this figure legend, the reader is referred to the web version of this article.)

**Table 3**
Elemental analysis results of selected points in Fig. 9b and Fig. 9d.

| Points analyzed | Zn (At%) | Cu (At%) | O (At%) | P (At%) | Ca (At%) | Ratio of Zn/Ca | Ratio of Ca/P |
|---|---|---|---|---|---|---|---|
| 1: Stent residual | 98.51 | 1.49 | – | – | – | – | – |
| 2: Degradation products | 32.12 | 1.21 | 66.16 | 0.40 | 0.10 | 321.20 | 0.25 |
| 3: Degradation products | 9.71 | 0.50 | 86.25 | 2.52 | 1.01 | 9.61 | 0.40 |
| 4: Tissue | 2.54 | – | 95.03 | 2.21 | 0.22 | – | – |
| 5: Degradation products | 37.30 | 0.91 | 60.47 | 1.12 | 0.20 | 186.50 | 0.18 |
| 6: Degradation products | 33.68 | 0.63 | 61.05 | 3.37 | 1.26 | 26.73 | 0.38 |
| 7: Degradation products | 21.11 | 0.70 | 58.35 | 12.30 | 7.54 | 2.80 | 0.61 |

**Table 4**
Zn accumulation in nearby tissues.

| Group | 6 months | | | 12 months | | | 24 months | | |
|---|---|---|---|---|---|---|---|---|---|
| | Proximal n1 = 6, n2 = 5 | Distal n1 = 6, n2 = 5 | Apex cordis n1 = n2 = 2 | Proximal n1 = n2 = 6 | Distal n1 = n2 = 6 | Apex cordis n1 = n2 = 2 | Proximal n1 = n2 = 5 | Distal n1 = n2 = 5 | Apex cordis n1 = n2 = 2 |
| Zn-Cu stented group (μg/g) | 53 ± 7 | 43 ± 15 | 31 ± 2 | 51 ± 5 | 53 ± 6 | 27 ± 2 | 52 ± 7 | 48 ± 10 | 28 ± 3 |
| $p_1$ | 0.2 | | | 0.5 | | | 0.6 | | |
| Negative control group (μg/g) | 45 ± 6 | 44 ± 13 | 27 ± 3 | 54 ± 2 | 52 ± 4 | 30 ± 7 | 50 ± 8 | 53 ± 3 | 30 ± 4 |
| $p_2$ | 0.1 | 0.7 | 0.4 | 0.3 | 0.9 | 0.8 | 0.6 | 0.9 | 0.7 |

$n_1$: samples of the Zn-Cu group, $n_2$: samples of the negative control group.
$p_1$: p values between the proximal and distal groups.
$p_2$: p values between the Zn-Cu and negative control groups.

the Zn-Cu stent can retain its integrity during crimping, inflation to nominal pressure, or even inflation to balloon burst. Additionally, no breakage or cracks were found on stents under these deformation processes.

The minimum radial strength of a stent should be is 175 mmHg (23.33 kPa) or 300 mmHg (40.00 kPa) with a safety factor [32]. With a radial strength of (114 ± 3) kPa (Fig. 2), the Zn-Cu stent can offer enough supporting force in the initial stage of post-implantation. The acute recoil of the Zn-Cu stent in porcine coronary arteries is also lower than that of the first commercialized biodegradable metal stent ((5.57 ± 0.72)% [33]) made of WE43 (a commercialized Mg-based alloy consisting of 93% Mg and 7% rare earth elements), which means the comprehensive mechanical performance of the Zn-Cu stent is acceptable for clinical use.

In this study, sixteen healthy female Shanghai white pigs were implanted with 40 Zn-Cu stents. The device success rate was 100%. No abnormal situation was observed during the operation (with electrocardiogram and blood pressure monitored), and no dissection, perforation, cardiac tamponade, or thrombus formation occurred early after implantation (within one month). Thus, the device usability and the acute safety of the Zn-Cu stent can be confirmed.

### 4.2. In vivo degradation properties of the Zn-Cu stents

Among the three candidates of biodegradable metals (Mg, Fe, and Zn), Mg and its alloys are extremely active and corrode too fast [34,35], whereas Fe and its alloys corrode too slow [36,37]. Zinc possesses a standard corrosion potential of −0.76 V vs. standard hydrogen electrode (SHE), which is intermediate between Fe (−0.44 V vs. SHE) and Mg (−2.37 V vs. SHE), intuitively enabling it to provide an intermediate degradation rate [38] between Fe and Mg. The near-ideal degradation rate has been considered one of the main advantages of the Zn-based stent [39].

The first commercialized Mg-based biodegradable metal stent AMS-1 was largely bio-absorbed into inorganic ions within 60 days of implantation in the porcine coronary artery [40] and fully degraded after 4 months of implantation in the human body [41]. As mechanical integrity is needed for at least 3–6 months [42], modifications of the Mg-based stent characteristics with prolonged degradation are still in development.

In the present work, the Zn-Cu stent retained its original integrity at the first 3 months of implantation in a porcine coronary artery (Fig. 4b), without any localized accumulations of degradation products. The degradation rate calculated from the (92 ± 1)% residual volume after the 3 months of implantation is approximately 0.016 mm/y. This is quite close to the benchmark [43] of an ideal degradation rate of 0.02 mm/y. The supporting units (Fig. S1, described in S1.2) of the Zn-Cu stent retained integrity at 6 months (Fig. 4c), which suggests that the Zn-Cu stent developed in this work can provide a long-enough supporting period for the arterial remodeling and healing.

Another major concern during the stent degradation process is the corrosion mode. Nonuniform corrosion may lead to the rapid loss of scaffolding function or the stent fracture at the early period of implantation. The stent fracture was usually associated with clinical target lesion revascularization [44], which may be a challenge for the biodegradable metal stents. In this study, the Zn-Cu stents maintained their mechanical integrity at 6 months without finding severe localized corrosion (Fig. 4c). Additionally, compact and continuous corrosion layers are observed in Fig. 4b and Fig. 4c, which means that the dominant corrosion type is still uniform corrosion after 6 months of implantation. As the endothelialization process could be completed during the first month post-surgery (shown in Fig. 6a and Fig. 8a), the stent fracture induced by the degradation process could not adversely affect the stented vessels.

Localized corrosion accumulation points were observed at 9 months (Fig. 4d). This indeed leads to a release of the stented vessel restriction. As a result, the MLD of the Zn-Cu stented vessels showed a gradually increased trend (positive reconstruction) from this time point (Fig. 7 and Table 2). A similar positive reconstruction of the PLLA stent implanted vessels has been reported in the porcine model [45]. At the endpoint of our test, the difference between the end point (24 months) and the 9 months' time point was significant (Fig. 7, $p < 0.05$).

Moreover, the restoration of pulsatility was believed to occur with the release of restriction to vessels [45]. The pulsatility restoration can recover important vessel functions such as the unimpeded vasomotion, which is critical to control blood flow and pressure [46]. The impairment of coronary vasomotion induced by the implantation of the permanent stent will last for a lifetime. The pulsatility restoration is a remarkable advantage of the biodegradable stent compared with that of the permanent stent. By contrast, the degradation products of iron appear to be stable in the physiological environment [47] and thus result in a long-term retention of the stented vessels like the permanent stent. Results of this study suggest that this disadvantage of the iron-based stent has been overcome by the Zn-Cu stent.

At the end of the test (24 months), the residue volume of the implanted Zn-Cu stent is only (28 ± 13)%. The degradation of the stent makes it invisible in the coronary angiography images (Fig. 3b) and OCT images (Fig. 8d–f). Evidence gathered in this study indicates that the Zn-Cu stent has the potential of being completely degraded after a longer time.

### 4.3. Biocompatibility of the Zn-Cu stent

#### 4.3.1. Effects of the element accumulation in the vascular vessel

The dietary allowance of Zn ranges from 2 mg/day for infants to 14 mg/day for adults [16], and the blood content of Zn is 32.3 mg/kg [48], which indicates that the amount of Zn induced by Zn-Cu stent implantation (approximately 25 mg) is too low to be accumulated in far-away organs. As shown in Table 4, Zn seems unli-

kely to accumulate in the apex cordis, located distal or proximal of stented artery segments. The rapid transfer rate of the ionic zinc in living tissue [49] may be the explanation of this result. The biocompatibility of the pure Zn implanted in arteries has also been proved in previous studies [6,50]. The dietary allowance of Cu ranges from 0.2 mg/day for infants to 1.3 mg/day for adults [16], and the $LD_{50}$ of $Cu^{2+}$ is 5.6 mg/kg (intraperitoneal injection, mice) [51]. Similar to the content of Zn, the content of Cu (0.2 mg) in a Zn-Cu stent is also far below the amount that can bring in systemic toxicity. Tang et al. [25] studied the cytocompatibility of Zn-xCu (x = 1, 2, 3, and 4 wt%), in which the Zn-3Cu shows a similar cell viability as that of pure Zn. The addition of 0.4 wt% Cu in the Zn-0.8Mn alloy can even significantly improve the L929 cell viability [12]. Many kinds of Cu-content alloys have been developed and studied *in vivo* for their antibacterial activity, while none of the biocompatibility issues have been found in these studies ([52,53]).

In our present work, normal tissues are observed around the strut residuals and the degradation products during the whole implantation period (Fig. 8 and Fig. 6, respectively), which suggests their good biocompatibility. On the contrary, adverse consequences were observed in an early study of iron-based implants, which generated a layered corrosion product and pushed away any biological matter to a distance >750 μm from the original implant surface after 9 months with little-to-no tissue integration [50]. Additionally, the rapid-re-endothelization process (within one month, Fig. 6a and Fig. 8a) also indicates that the existence of Cu has not brought in new biocompatibility problems.

Calcium phosphate crystals in the form of hydroxyapatite (HA) is an indicator of the atherosclerotic plaque [54], which is deeply unappealing after stenting. For the Mg-based stent, the average Ca/P ratio of the high Ca-containing degradation products after 4 and 12 months of implantation was close to 5/3 (the Ca/P ratio of HA) [55], which is a potential risk that cannot be ignored. In this study, even in the sequential degradation products of 18 months, the observed Ca/P ratio is only 0.61 (Table 3), which is still much lower than that of HA (1.67). Additionally, neither osteoblast-like SMC nor matrix vesicles were observed when the struts replaced by normal tissue (Fig. 6c-d3), which are indicators of the extracellular (ECM) mineralization and the SMC calcification [56]. This confirms that the Zn ions can decrease the crystallinity of the HA in the physiological environment [57], which might be another natural advantage in addition to the ideal degradation rate compared with Mg-based stents.

#### 4.3.2. Transport of the degradation products

The degradation mechanism of zinc was proposed by Yang et al. using a rabbit abdominal aorta model [6]. A precipitate containing Ca and P was found in the sequential degradation products, which is confirmed by the Ca and P peaks shown in Fig. 9. However, this is unlikely to induce accumulation of a large volume of undissolved degradation products *in situ* (Fig. 6d1–d3 and Fig. 8c–d). Additionally, Fig. 10d shows that the degradation products have diffused into the tissues nearby after 18 months of implantation. As described before, Zn ions can decrease the crystallinity of HA in the physiological environment. Zn can also prevent further growth of Ca-P phases by adsorbing onto their surfaces [57]. This may be the reason why the leaving parts of the degradation products have a quite small size (<20 μm) (Fig. 6d2). Thus, the degradation products are more likely to be moved. The co-occurrence of Zn and Cu peaks can be observed both in the strut and in the degradation product area (Fig. 9), which indicates the co-diffusion of the two elements.

The green circle shown in Fig. 6d3 highlighted one part of the degradation product with more than 10 cell nuclei around, which is the morphological characteristics of foreign body macrophages and foreign body giant cells. This result provides evidence for the cellular path of the degradation products' moving pathway. As shown in Fig. 6 and Fig. 9, the main moving direction of the degradation products is abluminal. This guaranteed that the strut is replaced by normal tissue during this process without the risk of entering the blood circulatory system and causing thrombosis or inflammation responses. The observed newborn endomembrane is smooth, and no thrombosis or severe inflammation response was found (Fig. 6 and Fig. 8). These results suggested that the transport of Zn-Cu stent degradation products is safe for the stented model.

### 4.4. Comprehensive comparison of recently reported biodegradable stents

We summarize the biodegradable behavior and the main medical device performance of different stents from previous reports on biodegradable stents in Table 5.

The wall thickness of the Zn-Cu stent is 100 μm, which is thinner than that of the biodegradable BVS (150 μm, made of PLLA) [39] and DREAMS 2G (140 μm, the clinically used Mg-based stent) [33]. A thinner wall is associated with the lower crossing profile (better deliverability) and lower rates of restenosis [58]. The lower acute recoil *in vivo* and the thinner wall together leads to a higher acute lumen gain, which is a key performance of the coronary stent [45,58].

As observed in Fig. 3a, the radiopacity of the Zn-Cu stent is clear enough for the stenting procedures. In contrast, Mg-based stents were almost invisible in the angiographic images [39]. Locating the Mg-based stent relied on radiopaque markers on the balloon. These markers, along with radiopaque iodinated contrast agents, enable the precise placement of the stent within the artery. However, once the deployment system was removed and the contrast agent dissipates, a stent with low radiopacity presents a problem if the stent later requires additional dilation [59]. Good radiopacity has a positive impact on the application prospect of zinc as a degradable stent.

The first clinical trial of the Mg-based stent (AMS-1, without drug-elution) was reported in *The Lancet* [41] in 2007. The faster degradation rate of the AMS-1 than the clinical requirement would induce restenosis and further reoperation rate [60]. During the last decade, two generations of commercialized drug-eluting Mg-based stents (DREAMS 1G and DREAMS 2G) have been developed to solve the problem. Positive clinical outcomes have been reported, and long-term observation of the DREAMS 2G is still ongoing. Further, because of their ultra-low radiopacity, the Mg-based stents cannot provide enough visibility when additional dilations are required during the stenting procedure [59]. This may remain as another major limitation for clinical use of the Mg-based stents.

On the other hand, far lower degradation rate than the clinical requirement was observed when the biodegradable iron stent was implanted into the native descending aorta of rabbit in 2001 [61]. The long-term existence of the iron stent in the blood vessel may further cause tissue inflammation and impairment. Recently, researchers developed ultrathin struts iron-based stents with appropriate mechanical properties to shorten degradation time. The zinc barrier layer makes it possible to maintain adequate scaffolding after 3 months and corrode after 13 months in rabbit models. However, complete bio-resorption of the degradation products has not been observed in their work, and the "gap" between the struts and the tissues, mentioned above, has also been observed after 3 months of implantation. Iron ions are easy to precipitate; thus, the elimination of the remaining degradation products is very slow [36]. This may be the reason why the restoration of the vessel vasomotion has been reported in the study of Mg-based stents [62] and PLLA stents [45] but not for the iron-based stents by far.

**Table 5**
Comprehensive comparison of recently reported biodegradable stents.

| Ref. and published years | Degradation behaviors | | | | | Medical device performance | | | |
|---|---|---|---|---|---|---|---|---|---|
| | Materials[!] | Material status and Models used[@] | | Degradation behaviors and main findings[#] | | Strut thickness[$] and radial strength | Crossing profile | Recoil[&] | Radiopacity[*] |
| Present work | Zn-0.8Cu | Stent | Porcine coronary artery | Retained (67 ± 13)% and (28 ± 13)% of stent volume after 12 and 24 months of implantation<br>Struts corroded replaced by normal tissues | a | 100 μm<br>(114 ± 3) kPa | (0.8–1.0) mm | (4 ± 3)% | + + + + + + + |
| 2017 [6] | Pure zinc | Stent | Rabbit abdominal aorta | Degraded (41.75 ± 29.72)% of stent volume after 12 months of implantation.<br>Struts corroded replaced by normal tissues | b | Not reported | Not reported | Not reported | Not reported |
| 2018 [62] DREAMS 2G | WE43 (93% Mg and 7% rare earth elements) | Stent with drug coating | Human coronary artery | Not reported | c | 140 μm<br>(197 ± 5) kPa [33] | 1.44 mm [33] | (5.57 ± 0.72)% [33] | Located by radiopaque markers in the stent<br>+ + |
| 2007 [41] AMS-1 | WE43 (93% Mg and 7% rare earth elements) | Stent | Human coronary artery | Stents can be safely degraded after 4 months | d | 165 μm [60] | 1.44 mm [33] | Luminal diameter 2.18 mm;<br>In-segment acute gain 1.41 mm | Located by radiopaque markers on the balloon<br>+ |
| 2018 [55] | Mg-Nd-Zn-Zr | Stent | Rabbit common carotid artery | Stent struts were mostly replaced *in situ* by degradation products in 4 months | e | 150 μm | Not reported | Not reported | Located by radiopaque markers on the balloon<br>+ |
| 2017 [47] | Nitrided iron | Stent | Tibet minipig coronary arteries | The nitrided iron scaffold has a higher corrosion rate than the pure iron scaffold and would probably completely corrode in 4–5 years | f | 70 μm<br>(171 ± 5) kPa [36] | (0.99 ± 0.02) mm [36] | Not reported | Not reported |
| 2016 [36] | Nitrided iron with a zinc barrier layer | Stent with a drug coating | Rabbit abdominal aorta | With a corrosion period of 13 months.<br>Corrosion particles are biostable up to 13 months | g | 53 μm struts with 24 μm coating<br>(123 ± 3) kPa | (1.04 ± 0.02) mm | Not reported | Not reported |
| 2001 [61] | Pure iron (>99.8% iron) | Stent | Rabbit native descending aorta | *In vitro* degradation rate is 1697 g/($m^2$ × h). Degradation rates *in vivo* were found to be slower than expected *in vitro* | h | (100–120) μm | Not reported | 2.2% | Not reported |
| 2006 [68] | Pure iron (>99.5% iron) | Stent with peripheral design | Minipig native descending aorta | Degradation of a stent produced from pure iron is slow, thereby preventing fragment embolization. A faster degradation rate is needed | i | Not reported | Not reported | Not reported | Not reported |

(*continued on next page*)

**Table 5** (*continued*)

| Ref. and published years | Degradation behaviors | | | | | Medical device performance | | | |
|---|---|---|---|---|---|---|---|---|---|
| | Materials[!] | Material status and Models used[@] | | Degradation behaviors and main findings[#] | | Strut thickness[$] and radial strength | Crossing profile | Recoil[&] | Radiopacity[*] |
| 2018 [67] NeoVas | PLLA | Stent with a drug coating | human | Haven't been observed yet | j | 160 μm backbone with 10 μm polymer | Not reported | Not reported | Located by radiopaque markers in the stent + + |
| 2017 [64] Absorb GT1 BVS | PLLA | Stent with a drug coating | human | Bio-resorption is complete in ~3 years | k | 150 μm [33] | (1.38 ± 0.01) mm [33] | (5.22 ± 0.38)% expansion into mock vessel [33] | Platinum markers + + |

!: The composition of the materials is given in wt.%. @: Large animal models have more cardiovascular similarities in terms of anatomy, physiology, and size to those of humans than to those of the rodent species; pigs have been used for decades to develop surgical procedures for implementation in humans [54]. #: The ideal corrosion rate is 0.02 mm/y [43]; the mechanical integrity of the stent is needed for 3–6 months [42]. $: Thinner struts induce greater deliverability, lower rates of restenosis [58], lesser injury, and better integration with the vessel wall [69]. &: Acute recoil is one of the most important determinants of the post-procedure severity of the residual lesion [70]. *: Radiopacity plays a key role when additional dilation is needed during the stenting procedure [59]. The radiopacity is related to the density of the materials and was represented by the amount "+" according to the reported material density [71]. NA: Not applicable.

(a) Both the initial and the subsequent corrosion products reached the maximum volume at 12 months and decreased gradually over the next 12 months. The subsequent corrosion products can be moved in the abluminal direction and the corroded place of the struts can be replaced by normal tissues. The stent retained its mechanical integrity for 6 months. The clinical device performance is comparable to that of the commercialized DES.

(b) No severe inflammation, platelet aggregation, thrombosis formation, or obvious intimal hyperplasia was observed at all time points after implantation. The uniform corrosion mode is dominant in the first 6 months, and the localized corrosion mode is dominant at 6 and 12 months. The stent retained its mechanical integrity for 6 months.

(c) Restoration of the vessel geometry, vasomotion, and bio-resorption signs were observed up to 12 months with preservation of the lumen size between 6 and 12 months.

(d) Absorbable metal stents are not visible in angiography. However, low radiolucency becomes an advantage when repeat assessments with computed tomography and magnetic resonance imaging are used to investigate the stented lesion, allowing noninvasive confirmation of patency.

(e) Results showed that the bare JDBM stent had good safety and efficacy with a complete re-endothelialization within 28 days.

(f) The corrosion products might contribute to radial strength when they are surrounded or connected by tissues. There were struts corroded completely into corrosion products after 12 months of implantation in a rabbit model, while nearly intact struts also exist after 53 months of implantation in a porcine model, which was induced by the localized corrosion behavior of the stents.

(g) Iron-based scaffold shows good clinical device performance comparable to that of a current mainstream drug-eluting coronary stent (Xience Prime). The abated corrosion particles induced the gap between the struts and tissues in 3 months of implantation. Corrosion particles are bio-stable up to 13 months, causing no adverse events or adverse effects to the local tissue.

(h) Iron-based stents (NOR-I) have a low thrombogenicity and cause only mild inflammatory response of the stented vessel without pronounced neointimal hyperplasia. They lack local or systemic toxicity.

(i) Histopathological examination of heart, lung, spleen, liver, kidney, and para-aortic lymphatic nodes demonstrated no signs of iron overload or iron-related organ toxicity. The loss of luminal diameter was not statistically different if iron-based stents were compared with 316-L stents.

(j) The NeoVas BRS was noninferior to CoCr-EES for the primary endpoint of 1-year angiographic in-segment LL and resulted in comparable 1-year clinical outcomes, including recurrent angina.

(k) BVS was associated with increased rates of composite device-oriented adverse events and device thrombosis cumulatively at 2 years and between 1 and 2 years of follow-up compared with EES.

Synthetic polymer is another branch of materials to fabricate the biodegradable (bioabsorbable) coronary stents [63]. The first commercialized polymer coronary stent is "Absorb GT1 BVS" (PLLA, approved by the FDA in July 2016). However, the FDA issued a safety alert for BVS in March 2017, and Abbott Vascular called a halt to the sale of this device only 18 months after approval. The main challenge for the PLLA stent is the very late scaffold thrombosis, which is beyond 1 year [64], and the most frightening aspect of very late scaffold thrombosis is the possible etiology linked to the intraluminal dismantling of the PLLA stent [65]. Furthermore, the thick wall of the PLLA stent is also associated with the device success rate, bringing in the limitation in case of device overlapping and side branch selection [66]. It has been found that BVS stents bring in more device thrombosis risks in small vessels [66]. Thus, reducing the scope of indications (such as the selection of appropriate target vessel diameter) may be a way out for the PLLA stents. Han et al. reported a 1-year randomized clinical trial in 2018, in which the PLLA stents had diameters ranging from 2.5 to 3.5 mm [67]. The device used (NeoVas, Lepu Medical, China) in this study has been approved by the China Food and Drug Administration on February 26, 2019, and long-term outcomes of the PLLA stents are expected.

As a newcomer, pure zinc was first considered to be a candidate biodegradable material for cardiovascular applications in 2013 [50]. However, the study just simply put the pure zinc wire in the rat abdominal aorta, without considering the actual stent structure and suitable large animal models.

The present work was carried out on a large animal model (i.e., pig). The stent, which was fabricated using a standardized stent production technique, was deployed in porcine coronary arteries. Large animal models have more cardiovascular similarities in terms of anatomy, physiology, and size to humans than to rodent species [54]. The results demonstrated that the Zn-Cu stent has sufficient mechanical properties and excellent radiopacity and degrades with a proper degradation rate without causing degradation product accumulation, thrombosis, or inflammatory responses after implantation up to 24 months; therefore, it has a great potential for further clinical applications.

## 5. Conclusions

The Zn-Cu stent degrades with a proper degradation rate, and after 24 months of implantation, it was approximately 28 ± 13 vol % of the stent remained. Degradation products can be moved in the abluminal direction by multinucleated giant cells, and the strut can be replaced by normal tissue during this process, without the risk of entering the circulatory system and causing other unforeseeable problems. The endothelialization process can complete within the first month of post-surgery, while thrombosis, localized necrosis, or serious inflammatory responses are not found even after implantation of up to 24 months. The addition of copper did not induce new risks associated with stent implantation. Results of the long-term *in vivo* study show that the Zn-0.8Cu coronary artery stent is promising for further clinical applications.

## Acknowledgments

This work was supported by the National Key Research & Development Program of China (No. 2016YFC1102500), the National Natural Science Foundation of China (No. 31700819), the Fundamental Research Funds for the Central Universities (No. 06500098), and the Young Elite Scientists Sponsorship Program by CAST (YESS, No. 2018QNRC001). As chief scientist, Professor Haijun-Zhang initiated the study and also participated in key details of the experimental processes.

## Disclosure

The Zn-Cu stent fabrication processes such as femtosecond laser cutting, acid pickling, chemical polishing, crimping, packaging, and EO sterilization processes were supported by Rientech MedTec Co., Ltd, which was one of the participants of the National Key Research & Development Program of China (No. 2016YFC1102500).

## Appendix A. Supplementary data

Supplementary data to this article can be found online at https://doi.org/10.1016/j.actbio.2019.08.012.

## References

[1] M. Vaez, M. Dalén, Ö. Friberg, J. Nilsson, O. Frøbert, B. Lagerqvist, T. Ivert, Regional differences in coronary revascularization procedures and outcomes: a nationwide 11-year observational study, Eur. Heart J. Qual. Care Clin. Outcomes 3 (3) (2017) 243–248.
[2] G. Pamela, D. Nicolas, B. Nicolas, R.J. Van, L. Thibault, B. Antonio, C. Didier, Incomplete stent apposition and very late stent thrombosis after everolimus eluting stent implantation and dual antiplatelet therapy interruption. A case of OCT guided therapy, Int. J. Cardiol. 180 (2015) 52–54.
[3] A. Farb, D.K. Weber, F.D. Kolodgie, A.P. Burke, R. Virmani, Morphological predictors of restenosis after coronary stenting in humans, Circulation 105 (25) (2002) 2974–2980.
[4] S. Cassese, R.A. Byrne, G. Ndrepepa, S. Kufner, J. Wiebe, J. Repp, H. Schunkert, M. Fusaro, T. Kimura, A. Kastrati, Everolimus-eluting bioresorbable vascular scaffolds versus everolimus-eluting metallic stents: a meta-analysis of randomised controlled trials, Lancet 387 (10018) (2015) 537–544.
[5] A.V. Finn, R. Virmani, The clinical challenge of disappearing stents, Lancet 387 (10018) (2016) 510–512.
[6] H. Yang, C. Wang, C. Liu, H. Chen, Y. Wu, J. Han, Z. Jia, W. Lin, D. Zhang, W. Li, W. Yuan, H. Guo, H. Li, G. Yang, D. Kong, D. Zhu, K. Takashima, L. Ruan, J. Nie, X. Li, Y. Zheng, Evolution of the degradation mechanism of pure zinc stent in the one-year study of rabbit abdominal aorta model, Biomaterials 145 (2017) 92–105.
[7] M.A. Saghiri, A. Asatourian, J. Orangi, C.M. Sorenson, N. Sheibani, Functional role of inorganic trace elements in angiogenesis-Part II: Cr, Si, Zn, Cu, and S, Crit. Rev. Oncol. Hematol. 96 (1) (2015) 143–155.
[8] M. Purushothaman, R. Gudrun, T. Michal, H. Bernhard, Zinc modulates PPARγ signaling and activation of porcine endothelial cells, J. Nutr. 133 (10) (2003) 3058.
[9] T. Kaji, Y. Fujiwara, C. Yamamoto, M. Sakamoto, H. Kozuka, Stimulation by zinc of cultured vascular endothelial cell proliferation: possible involvement of endogenous basic fibroblast growth factor, Life Sci. 55 (23) (1994) 1781.
[10] P.J. Little, R. Bhattacharya, A.E. Moreyra, I.L. Korichneva, Zinc and cardiovascular disease, Nutrition 26 (11) (2010) 1050–1057.
[11] H. Li, H. Yang, Y. Zheng, F. Zhou, K. Qiu, X. Wang, Design and characterizations of novel biodegradable ternary Zn-based alloys with IIA nutrient alloying elements Mg, Ca and Sr, Mater. Des. 83 (2015) 95–102.
[12] Z. Shi, J. Yu, X. Liu, H. Zhang, D. Zhang, Y. Yin, L. Wang, Effects of Ag, Cu or Ca addition on microstructure and comprehensive properties of biodegradable Zn-0.8Mn alloy, Mater. Sci. Eng. C: Mater. Biol. Appl. 99 (2019) 969–978.
[13] X. Tong, D. Zhang, X. Zhang, Y. Su, Z. Shi, K. Wang, J. Lin, Y. Li, J. Lin, C. Wen, Microstructure, mechanical properties, biocompatibility, and in vitro corrosion and degradation behavior of a new Zn-5Ge alloy for biodegradable implant materials, Acta Biomater. 82 (2018) 197–204.
[14] J. Venezuela, M.S. Dargusch, The influence of alloying and fabrication techniques on the mechanical properties, biodegradability and biocompatibility of zinc: a comprehensive review, Acta Biomater. 87 (2019) 1–40.
[15] X. Wang, X. Shao, T. Dai, F. Xu, J.G. Zhou, G. Qu, L. Tian, B. Liu, Y. Liu, In vivo study of the efficacy, biosafety, and degradation of a zinc alloy osteosynthesis system, Acta Biomater. 92 (2019) 351–361.
[16] P. Trumbo, A.A. Yates, S. Schlicker, M. Poos, Dietary reference intakes: vitamin A, vitamin K, arsenic, boron, chromium, copper, iodine, iron, manganese, molybdenum, nickel, silicon, vanadium, and zinc, J. Am. Diet. Assoc. 101 (3) (2001) 294–301.
[17] C.K. Sen, S. Khanna, M. Venojarvi, P. Trikha, E.C. Ellison, T.K. Hunt, S. Roy, Copper-induced vascular endothelial growth factor expression and wound healing, Am. J. Physiol. Heart Circ. Physiol. 282 (5) (2002) H1821.
[18] M. Yoshiaki, U. Takafumi, Y. Shinji, S. Ken-ichiro, S. Yusuke, Coronary endothelial dysfunction distal to stent of first-generation drug-eluting stents, JACC Cardiovasc. Interv. 5 (9) (2012) 966–973.
[19] V. Schächinger, M.B. Britten, A.M. Zeiher, Prognostic impact of coronary vasodilator dysfunction on adverse long-term outcome of coronary heart disease, Circulation 101 (16) (2000) 1899–1906.
[20] C. Liu, X. Fu, H. Pan, P. Wan, L. Wang, L. Tan, K. Wang, Y. Zhao, K. Yang, P.K. Chu, Biodegradable Mg-Cu alloys with enhanced osteogenesis, angiogenesis, and long-lasting antibacterial effects, Sci. Rep. 6 (2016) 27374.

[21] H. Chouirfa, H. Bouloussa, V. Migonney, C. Falentin-Daudre, Review of titanium surface modification techniques and coatings for antibacterial applications, Acta Biomater. 83 (2019) 37–54.
[22] J. Li, D. Zhai, F. Lv, Q. Yu, H. Ma, J. Yin, Z. Yi, M. Liu, J. Chang, C. Wu, Preparation of copper-containing bioactive glass/eggshell membrane nanocomposites for improving angiogenesis, antibacterial activity and wound healing, Acta Biomater. 36 (2016) 254–266.
[23] L.B. Romero-Sanchez, M. Mari-Beffa, P. Carrillo, M.A. Medina, A. Diaz-Cuenca, Copper-containing mesoporous bioactive glass promotes angiogenesis in an in vivo zebrafish model, Acta Biomater. 68 (2018) 272–285.
[24] A. Bari, N. Bloise, S. Fiorilli, G. Novajra, M. Vallet-Regi, G. Bruni, A. Torres-Pardo, J.M. Gonzalez-Calbet, L. Visai, C. Vitale-Brovarone, Copper-containing mesoporous bioactive glass nanoparticles as multifunctional agent for bone regeneration, Acta Biomater. 55 (2017) 493–504.
[25] Z. Tang, J. Niu, H. Huang, H. Zhang, J. Pei, J. Ou, G. Yuan, Potential biodegradable Zn-Cu binary alloys developed for cardiovascular implant applications, J. Mech. Behav. Biomed. Mater. 72 (2017) 182–191.
[26] Z. Shi, J. Yu, X. Liu, L. Wang, Fabrication and characterization of novel biodegradable Zn-Mn-Cu alloys, J. Mater. Sci. 34 (6) (2018) 1008–1015.
[27] J. Mazhar, E. Shaw, U.K. Allahwala, G.A. Figtree, R. Bhindi, Comparison of two dimensional quantitative coronary angiography (2D-QCA) with optical coherence tomography (OCT) in the assessment of coronary artery lesion dimensions, Int. J. Cardiol. Heart Vasc. 7 (2015) 14–17.
[28] R.W. Harrison, V. Radhakrishnan, J.C. Allen Jr., P.S. Lam, D.J. Allocco, S. Brar, M. Fahy, Z. Zhang, R. Fisher, F. Ikeno, P. Genereux, T. Kimura, M. Liu, W.K. Lye, H. Nagai, Y. Suzuki, R. White, M.W. Krucoff, The East-West late lumen loss study: comparison of angiographic late lumen loss between Eastern and Western drug-eluting stent study cohorts, Am. Heart J. 206 (2018) 61–71.
[29] H. Zhao, J.V. Humbeeck, Electrochemical polishing of 316L stainless steel slotted tube coronary stents, J. Mater. Sci. - Mater. Med. 13 (2002) 911–916.
[30] A. Shahryari, F. Azari, H. Vali, S. Omanovic, The response of fibrinogen, platelets, endothelial and smooth muscle cells to an electrochemically modified SS316LS surface: towards the enhanced biocompatibility of coronary stents, Acta Biomater. 6 (2) (2010) 695–701.
[31] S. Habibzadeh, L. Li, D. Shum-Tim, E.C. Davis, S. Omanovic, Electrochemical polishing as a 316L stainless steel surface treatment method: towards the improvement of biocompatibility, Corros. Sci. 87 (2014) 89–100.
[32] K.F.H.G.M. Agrawal, D.A. Leopold, H.G. Clark, Evaluation of poly(L-lactic acid) as a material for intravascular polymeric stents, Biomaterials 13 (1992) 176–182.
[33] W. Schmidt, P. Behrens, C. Brandt-Wunderlich, S. Siewert, N. Grabow, K.-P. Schmitz, In vitro performance investigation of bioresorbable scaffolds – standard tests for vascular stents and beyond, Cardiovasc. Revasc. Med. 17 (6) (2016) 375–383.
[34] F. Witte, Reprint of: The history of biodegradable magnesium implants: a review, Acta Biomater. 23 (Suppl) (2015) S28–S40.
[35] J. Liu, Y. Lin, D. Bian, M. Wang, Z. Lin, X. Chu, W. Li, Y. Liu, Z. Shen, Y. Liu, Y. Tong, Z. Xu, Y. Zhang, Y. Zheng, In vitro and in vivo studies of Mg-30Sc alloys with different phase structure for potential usage within bone, Acta Biomater. (2019), https://doi.org/10.1016/j.actbio.2019.03.009.
[36] W. Lin, D. Zhang, G. Zhang, H. Sun, H. Qi, L. Chen, Z. Liu, R. Gao, W. Zheng, Design and characterization of a novel biocorrodible iron-based drug-eluting coronary scaffold, Mater. Des. 91 (2016) 72–79.
[37] S. Loffredo, C. Paternoster, D. Mantovani, Iron-Based Degradable Implants, Encycl. Biomed. Eng. (2019) 374–385.
[38] J. Cheng, B. Liu, Y.H. Wu, Y.F. Zheng, Comparative in vitro study on pure metals (Fe, Mn, Mg, Zn and W) as biodegradable metals, J. Mater. Sci. 29 (7) (2013) 619–627.
[39] S.H. Im, Y. Jung, S.H. Kim, Current status and future direction of biodegradable metallic and polymeric vascular scaffolds for next-generation stents, Acta Biomater. 60 (2017) 3–22.
[40] R. Waksman, R. Pakala, P.K. Kuchulakanti, R. Baffour, D. Hellinga, R. Seabron, F. O. Tio, E. Wittchow, S. Hartwig, C. Harder, Safety and efficacy of bioabsorbable magnesium alloy stents in porcine coronary arteries, Catheter. Cardiovasc. Interv. 68 (4) (2006) 607–617.
[41] R. Erbel, M.C. Di, J. Bartunek, J. Bonnier, B.B. De, F.R. Eberli, P. Erne, M. Haude, B. Heublein, M. Horrigan, Temporary scaffolding of coronary arteries with bioabsorbable magnesium stents: a prospective, non-randomised multicentre trial, Lancet 369 (9576) (2007) 1869–1875.
[42] M. Moravej, D. Mantovani, Biodegradable metals for cardiovascular stent application: interests and new opportunities, Int. J. Mol. Sci. 12 (7) (2011) 4250–4270.
[43] F. Witte, N. Hort, F. Feyerabend, C. Vogt, Magnesium (Mg) Corrosion: a Challenging Concept for Degradable Implants, Corros. Magnesium Alloys, Woodhead Publishing Ltd, 2011, pp. 403–425.
[44] S. Kuramitsu, M. Iwabuchi, H. Yokoi, T. Domei, S. Sonoda, T. Hiromasa, T. Morinaga, Y. Kobayashi, K. Ohe, K. Goya, K. Yamaji, M. Hyodo, Y. Soga, K. Kondo, S. Shirai, K. Ando, K. Sakai, M. Nobuyoshi, Incidence and clinical impact of stent fracture after the Nobori biolimus-eluting stent implantation, J. Am. Heart Assoc. 3 (2) (2014) e000703.
[45] J.P. Lane, L.E. Perkins, A.J. Sheehy, E.J. Pacheco, M.P. Frie, B.J. Lambert, R.J. Rapoza, R. Virmani, Lumen gain and restoration of pulsatility after implantation of a bioresorbable vascular scaffold in porcine coronary arteries, JACC Cardiovasc. Interv. 7 (6) (2014) 688–695.
[46] Y. Sotomi, Y. Onuma, C. Collet, E. Tenekecioglu, R. Virmani, N. Kleiman, P. Serruys, Bioresorbable scaffold: the emerging reality and future directions, Circ. Res. 120 (8) (2017) 1341–1352.
[47] W. Lin, L. Qin, H. Qi, D. Zhang, G. Zhang, R. Gao, H. Qiu, Y. Xia, P. Cao, X. Wang, W. Zheng, Long-term in vivo corrosion behavior, biocompatibility and bioresorption mechanism of a bioresorbable nitrided iron scaffold, Acta Biomater. 54 (2017) 454–468.
[48] W.G. Eggleton, The zinc and copper contents of the organs and tissues of Chinese subjects, Biochem. J. 34 (7) (1940) 991.
[49] L. Xu, G. Yu, E.F. Pan, K. Yang, In vivo corrosion behavior of Mg-Mn-Zn alloy for bone implant application, J. Biomed. Mater. Res. A 83A (3) (2007) 703–711.
[50] P.K. Bowen, J. Drelich, J. Goldman, Zinc exhibits ideal physiological corrosion behavior for bioabsorbable stents, Adv. Mater. 25 (18) (2013) 2577–2582.
[51] M.M. Jones, J.E. Schoenheit, A.D. Weaver, Pretreatment and heavy metal LD50 values, Toxicol. Appl. Pharmacol. 49 (1) (1979) 41–44.
[52] X. Wang, H. Dong, J. Liu, G. Qin, D. Chen, E. Zhang, In vivo antibacterial property of Ti-Cu sintered alloy implant, Mater. Sci. Eng. C: Mater. 100 (2019) 38–47.
[53] Y. Li, L. Liu, P. Wan, Z. Zhai, Z. Mao, Z. Ouyang, D. Yu, Q. Sun, L. Tan, L. Ren, Z. Zhu, Y. Hao, X. Qu, K. Yang, K. Dai, Biodegradable Mg-Cu alloy implants with antibacterial activity for the treatment of osteomyelitis: in vitro and in vivo evaluations, Biomaterials 106 (2016) 250–263.
[54] H.G. Tsang, N.A. Rashdan, C.B. Whitelaw, B.M. Corcoran, K.M. Summers, V.E. MacRae, Large animal models of cardiovascular disease, Cell Biochem. Funct. 34 (3) (2016) 113–132.
[55] J. Zhang, H. Li, W. Wang, H. Huang, J. Pei, H. Qu, G. Yuan, Y. Li, The degradation and transport mechanism of a Mg-Nd-Zn-Zr stent in rabbit common carotid artery: a 20-month study, Acta Biomater. 69 (2018) 372–384.
[56] J.A. Leopold, Vascular calcification: mechanisms of vascular smooth muscle cell calcification, Trends Cardiovasc. Med. 25 (4) (2015) 267–274.
[57] R.Z. LeGeros, C.B. Bleiwas, M. Retino, R. Rohanizadeh, J.P. LeGeros, Zinc effect on the in vitro formation of calcium phosphates- Relevance to clinical inhibition of calculus formation, Am. J. Dent. 12 (2) (1999) 65–71.
[58] A.C. Morton, D. Crossman, J. Gunn, The influence of physical stent parameters upon restenosis, Pathol. Biol. 52 (4) (2004) 196–205.
[59] C.H. Craig, C.M. Friend, M.R. Edwards, L.A. Cornish, N.A. Gokcen, Mechanical properties and microstructure of platinum enhanced radiopaque stainless steel (PERSS) alloys, J. Alloys Compd. 361 (2003) 187–199.
[60] C. Campos, T. Muramatsu, J. Iqbal, Y.-J. Zhang, Y. Onuma, H. Garcia-Garcia, M. Haude, P. Lemos, B. Warnack, P. Serruys, Bioresorbable drug-eluting magnesium-alloy scaffold for treatment of coronary artery disease, Int. J. Mol. Sci. 14 (12) (2013) 24492–24500.
[61] M.P. Wohlsein, M.J.H. Brugmann, A novel approach to temporary stenting: degradable cardiovascular stents produced from corrodible metal - results 6–18 months after implantation into New Zealand white rabbits, Heart 86 (5) (2001) 563–569.
[62] H.M. Garcia-Garcia, M. Haude, K. Kuku, A. Hideo-Kajita, H. Ince, A. Abizaid, R. Tölg, P.A. Lemos, C. von Birgelen, E.H. Christiansen, W. Wijns, J. Escaned, J. Dijkstra, R. Waksman, In vivo serial invasive imaging of the second-generation drug-eluting absorbable metal scaffold (Magmaris — DREAMS 2G) in de novo coronary lesions: insights from the BIOSOLVE-II first-in-man trial, Int. J. Cardiol. 255 (2018) 22–28.
[63] T.R. Welch, A.W. Nugent, S.R. Veeram Reddy, Biodegradable stents for congenital heart disease, Interv. Cardiol. Clin. 8 (1) (2019) 81–94.
[64] Z.A. Ali, P.W. Serruys, T. Kimura, R. Gao, S.G. Ellis, D.J. Kereiakes, Y. Onuma, C. Simonton, Z. Zhang, G.W. Stone, 2-Year outcomes with the absorb bioresorbable scaffold for treatment of coronary artery disease: a systematic review and meta-analysis of seven randomised trials with an individual patient data substudy, Lancet 390 (10096) (2017) 760–772.
[65] L. Raber, S. Brugaletta, K. Yamaji, C.J. O'Sullivan, S. Otsuki, T. Koppara, M. Taniwaki, Y. Onuma, X. Freixa, F.R. Eberli, P.W. Serruys, M. Joner, M. Sabate, S. Windecker, Very late scaffold thrombosis: intracoronary imaging and histopathological and spectroscopic findings, J. Am. Coll. Cardiol. 66 (17) (2015) 1901–1914.
[66] T. Kimura, What have we learned from the ABSORB trials?, JACC Cardiovasc Interv. 11 (3) (2018) 273–274.
[67] Y. Han, B. Xu, G. Fu, X. Wang, K. Xu, C. Jin, L. Tao, L. Li, Y. Hou, X. Su, Q. Fang, L. Chen, H. Liu, B. Wang, Z. Yuan, C. Gao, S. Zhou, Z. Sun, Y. Zhao, C. Guan, G.W. Stone, I. NeoVas randomized controlled trial, a randomized trial comparing the NeoVas sirolimus-eluting bioresorbable scaffold and metallic everolimus-eluting stents, JACC Cardiovasc. Interv. 11 (3) (2018) 260–272.
[68] M. Peuster, C. Hesse, T. Schloo, C. Fink, P. Beerbaum, C. von Schnakenburg, Long-term biocompatibility of a corrodible peripheral iron stent in the porcine descending aorta, Biomaterials 27 (28) (2006) 4955–4962.
[69] N. Foin, R.D. Lee, R. Torii, J.L. Guitierrez-Chico, A. Mattesini, S. Nijjer, S. Sen, R. Petraco, J.E. Davies, C. Di Mario, M. Joner, R. Virmani, P. Wong, Impact of stent strut design in metallic stents and biodegradable scaffolds, Int. J. Cardiol. 177 (3) (2014) 800–808.
[70] T. Ota, H. Ishii, T. Sumi, T. Okada, H. Murakami, S. Suzuki, K. Kada, N. Tsuboi, T. Murohara, Impact of coronary stent designs on acute stent recoil, J. Cardiol. 64 (5) (2014) 347–352.
[71] M.P. Staiger, A.M. Pietak, J. Huadmai, G. Dias, Magnesium and its alloys as orthopedic biomaterials: a review, Biomaterials 27 (9) (2006) 1728–1734.